Techset Composition Ltd, Salisbury
Doc: //techsetserver2/journal/IEE/COM/Articles/pagination/COM20150702.3d

IET Communications

Research Article

IET Journals
The Institution of Engineering and Technology

Q1 Performance analysis of orthogonal frequency division multiplexing systems in dispersive indoor power line channels inflicting asynchronous impulsive noise

ISSN 1751-8628
Received on 25th July 2015
Revised on 11th November 2015
Accepted on 5th December 2015
doi: 10.1049/iet-com.2015.0702
www.ietdl.org

Q2 *Hongming Zhang, Lie-Liang Yang, Lajos Hanzo* ✉

School of Electronics and Computer Science, University of Southampton, SO17 1BJ, UK
✉ *E-mail: lh@ecs.soton.ac.uk*

Abstract: Hidden semi-Markov modelling of the asynchronous impulsive noise (IN) encountered in indoor broadband power line communications (PLCs) is investigated by considering the statistical distributions of both the inter-arrival time and the duration of asynchronous IN components. Then, the bit error ratio (BER) of orthogonal frequency division multiplexing systems using Q-ary quadrature amplitude modulation is analysed with the aid of the proposed noise model, when communicating over dispersive indoor power line channels inflicting asynchronous IN in addition to the background noise. The authors' simulation results confirm the accuracy of the analysis and quantify the impact of various factors on the achievable BER performance. The grave impact of asynchronous IN on indoor broadband PLCs suggests that efficient techniques have to be designed for mitigating its effects.

1 Introduction

Power line communication (PLC) is one of attractive candidates for the so-called 'last mile' communications due to its cost efficiency, since it exploits the existing grid structure [1]. However, since the electrical supply networks have not been designed for data transmissions, they constitute a hostile propagation environment [2], where the multipath-induced dispersion and the impulsive noise (IN) are the two fundamental impediments in the way of high-integrity communications. Nonetheless, multicarrier comm unication techniques are capable of mitigating the multipath effects in PLC, whilst spreading the effects of IN over all subcarriers [3]. A range of advanced techniques were also reported in [4–6].

As a further impairment, the attenuation encountered in PLC is the result of the skin effect and dielectric losses [7]. By contrast, dispersive multipath signal propagation in PLC is caused by the mismatch of the impedance between a transmitter and its corresponding receiver [8]. As a result, a transmitted symbol may be spread over several adjacent symbols at the receiver, imposing inter-symbol interference (ISI), which was investigated in [8–10]. Furthermore, the statistical characteristics of ISI-contaminated power line channels were studied in [11–15].

In PLC, the noise can usually be classified into two categories: background noise and IN [16, 17]. The IN is typically characterised by the duration, inter-arrival time and power of its components [16]. According to its behaviour with respect to the mains cycle, IN can be classified into three types, namely the periodic mains-synchronous IN, the periodic IN that is asynchronous with the mains, as well as the asynchronous IN [16], which is mainly caused by the connection and disconnection of electrical devices. Typically, the asynchronous IN is the most dominant impairment of broadband PLCs due to its high power and unpredictable nature. Therefore, we focus our attention on the asynchronous IN in this treatise. Several studies demonstrated [16, 18, 19] that the average duration of IN bursts in PLC is relatively long in comparison to the IN bursts of wireless communications. More specifically, the measurement results of [16] showed that the average duration of the asynchronous IN bursts in PLC varies between tens of microseconds and tens of milliseconds. By contrast, in wireless communications, the duration of IN bursts is usually less than 0.1 μs [20]. These observations in turn imply that if signal samples with a symbol-duration of say 10 ns are transmitted at a Nyquist-rate of 100 MBaud, then more than 10^3 successive symbols may be corrupted by an IN burst, once it occurs. By contrast, in wireless communications, no more than ten successive samples are impaired by an IN burst. Naturally, these long impulsive bursts may inflict bursts of errors. As a result, the system's performance may be severely degraded, especially in high data-rate transmissions relying on short symbol durations. In the literature, two special cases of the multi-component Gaussian mixture model [21] have been used for modelling the IN, which are respectively referred to as the Bernoulli–Gaussian model [22] and the Middleton Class A model [23]. Specifically, in [3], the classic Poisson process was employed for evaluating the probability of IN occurrences, where the Bernoulli–Gaussian model was assumed. In [24], Markov chains were introduced for calculating the so-called impulsive index of the Middleton Class A model. However, in the above-mentioned pair of models the IN samples were independently generated, which fails to reflect the typical bursty behaviour of IN in PLC.

To mimic the bursty behaviour of IN, Markov chains were employed in [16, 25, 26]. In [16], a so-called partitioned Markov chain, which considered a set of IN-free states and a set of impulsive states were employed for modelling the bursty behaviour of IN. Later in [25], a two-state Markov chain model was adopted for mimicking the bursty nature of IN. In this model, the noise samples were generated as white Gaussian noise, where noise samples having an increased variance were generated to represent IN. Recently, a more accurate four-state Markov chain model was proposed [26], where the IN samples were assumed to obey the Middleton Class A model of [23]. Although these Markov chain-based noise models succeeded in generating bursty IN, the statistical accuracy of the state durations was not carefully considered.

Against this background, our new contribution is that the hidden semi-Markov model (HSMM) [27], which was shown to accurately model the duration of burst events in [28], is applied for modelling the bursty behaviour of asynchronous IN, when analytically characterising the bit error ratio (BER) performance of orthogonal frequency division multiplexing (OFDM)-based PLC systems using Q-ary quadrature amplitude modulation (QAM). Our simulation results verify the accuracy of our analytical results.

The rest of the paper is organised as follows. In Section 2, we describe the system and introduce our noise model. Section 3 details our analysis of the OFDM system considered. In Section 4, our closed-form BER expression is derived, while in Section 5 our analytical and simulation results are compared. Finally, we offer our conclusions in Section 6.

2 System and noise modelling

2.1 OFDM signalling

We consider a discrete-time baseband equivalent model of the OFDM system, which is illustrated in Fig. 1. In the OFDM system, a block of Q-ary QAM symbols is serial-to-parallel converted and then the parallel symbols $\boldsymbol{X} = [X_0, X_1, \ldots, X_{M-1}]^{\mathrm{T}}$ are modulated with the aid of inverse fast Fourier transform (IFFT), yielding the time-domain (TD) signals $\boldsymbol{x} = [x_0, x_1, \ldots, x_{M-1}]^{\mathrm{T}}$, which can be expressed as

$$\boldsymbol{x} = \mathcal{F}^{\mathrm{H}}\boldsymbol{X}, \tag{1}$$

where $\mathcal{F}$ is the normalised discrete Fourier transform (DFT) matrix [29] satisfying $\mathcal{F}\mathcal{F}^{\mathrm{H}} = \mathcal{F}^{\mathrm{H}}\mathcal{F} = \boldsymbol{I}_M$. Hence, $\mathcal{F}$ is an orthonormal matrix. After concatenating the cyclic prefix (CP), the TD transmitted symbols are arranged in the form of

$$\tilde{\boldsymbol{x}} = [x_{M-L'}, x_{M-L'+1}, \ldots, x_{M-1}, x_0, x_1, \ldots, x_{M-1}]^{\mathrm{T}}, \tag{2}$$

where L' is the length of the CP.

In OFDM systems, the bandwidth of each subchannel is usually significantly smaller than the coherence bandwidth of the communication channel. Hence, each of the subcarriers experiences flat fading. Therefore, after removing the CP at the receiver, the received baseband equivalent observations $\boldsymbol{y} = [y_0, y_1, \ldots, y_{M-1}]^{\mathrm{T}}$ can be formulated as

$$\boldsymbol{y} = \widetilde{\boldsymbol{H}}\boldsymbol{x} + \boldsymbol{n}, \tag{3}$$

where $\widetilde{\boldsymbol{H}}$ is an $(M \times M)$-element circulant matrix, which can be diagonalised by the DFT matrix, giving $\widetilde{\boldsymbol{H}} = \mathcal{F}^{\mathrm{H}}\boldsymbol{H}\mathcal{F}$, where $\boldsymbol{H}$ is a diagonal matrix. In (3), $\boldsymbol{n}$ is the noise vector, which includes both the Gaussian background noise and the IN, as it will be detailed in Section 2.3.

Assuming that perfect synchronisation has been achieved at the receiver, the decision variables can be obtained with the aid of the fast Fourier transform (FFT) operation as

$$\begin{aligned}\widetilde{\boldsymbol{X}} &= \mathcal{F}\boldsymbol{y} = \mathcal{F}(\widetilde{\boldsymbol{H}}\boldsymbol{x} + \boldsymbol{n}) = \mathcal{F}(\widetilde{\boldsymbol{H}}\mathcal{F}^{\mathrm{H}}\boldsymbol{X} + \boldsymbol{n}) \\ &= \mathcal{F}\mathcal{F}^{\mathrm{H}}\boldsymbol{H}\mathcal{F}\mathcal{F}^{\mathrm{H}}\boldsymbol{X} + \mathcal{F}\boldsymbol{n} = \boldsymbol{H}\boldsymbol{X} + \boldsymbol{N},\end{aligned} \tag{4}$$

where we have $\boldsymbol{N} = \mathcal{F}\boldsymbol{n}$. Furthermore, we assume that the phase rotations in $\boldsymbol{H}$ have been perfectly compensated by the coherent detection scheme. Then, based on (4), the transmitted symbols in $\boldsymbol{X}$ can be detected according to the decision rules of Q-ary QAM [30], where the detection performance is affected by both the channel attenuations in $\boldsymbol{H}$ and the noise samples in $\boldsymbol{N}$.

2.2 Modelling of indoor power line channels

Due to the frequent connection and disconnection of various types of loads, as well as the presence of cable branches, indoor PLC channels exhibit a time-variant frequency-selective channel transfer function (CTF). However, we can usually assume that the channel remains constant during a single OFDM symbol. This assumption is reasonable, since in high-speed data transmissions the PLC channels vary rather slowly. Furthermore, in contrast to wireless multipath channels, the multipath effect of PLC channels can be analytically calculated [9] with the aid of the CTF between any two outlets. According to [8], the CTF of the PLC channels can be expressed as

$$H(f) = \sum_{i=0}^{L_e-1} g_i \, \mathrm{e}^{-\alpha(f)v_p\tau_i} \, \mathrm{e}^{-\mathrm{j}2\pi f\tau_i}, \tag{5}$$

where L_e denotes the number of non-negligible paths; $|g_i| < 1$ is the reflection factor, which is determined both by the number of discontinuities included in the ith path, as well as by the reflection coefficient and the transmission coefficient of the ith path [9]; $\alpha(f)$ is a frequency-dependent attenuation factor, which is related both to the dielectric losses and ohmic losses [18]; and finally, τ_i is the delay of the ith reflected path, while v_p is the phase velocity. Correspondingly, the channel impulse response (CIR) can be formulated as $h(t) = \mathcal{F}^{-1}\{H(f)\}$, where $\mathcal{F}^{-1}\{x\}$ denotes the inverse Fourier transform of x. Note that the channel model expressed in (5) uses a top-down approach for modelling the PLC channels, where the associated values of the parameters can be obtained from measurements [8].

Specifically, when the OFDM signals of (2) are transmitted over the PLC channel characterised by (5), and the received signals are sampled at intervals of $\Delta t = T_{\mathrm{s}}M$ representing the chip duration, with T_{s} being the OFDM symbol duration, the chip-sampled baseband equivalent CIR after filtering can be expressed as $\boldsymbol{h} = [h_0, h_1, \ldots, h_{L-1}]^{\mathrm{T}}$, where $L \simeq \tau_{L_{e-1}}\Delta t$ is the discretised length of

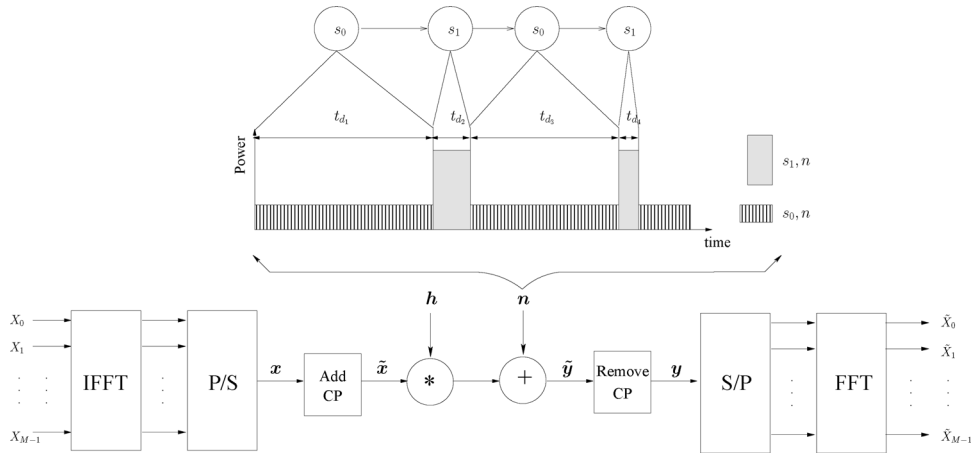

Fig. 1 *System and noise model. s_0: state without IN; s_1: state with IN. t_d: duration time of state s_i ($i = 0, 1$)*

the delay spread, which is an integer multiple of the chip-duration. Upon carrying out the FFT, the fading gains of the M subcarriers, which are denoted by $\boldsymbol{h}_f = [H_0, H_1, \ldots, H_{M-1}]^{\mathrm{T}}$, can be expressed as

$$\boldsymbol{h}_f = \sqrt{M}\mathcal{F}\boldsymbol{h}_M, \tag{6}$$

where we have $\boldsymbol{h}_M = [\boldsymbol{h}^{\mathrm{T}}, \boldsymbol{0}_{1\times(M-L)}]^{\mathrm{T}}$. Consequently, the diagonal matrix $\boldsymbol{H}$ seen in (4) is given by $\boldsymbol{H} = \mathrm{diag}\{H_0, H_1, \ldots, H_{M-1}\}$.

2.3 Noise modelling

The HSMM [27] is an extension of the classic hidden Markov model [31], where the underlying stochastic process obeys a semi-Markov chain, while the different states may have different durations [28]. Based on the HSMM, below we show a noise model for PLC.

As shown in Fig. 1, the noise contaminating the TD OFDM signals has two states, where s_0 represents the sole presence of the Gaussian background noise, while s_1 represents the presence of both the Gaussian background noise and IN. Explicitly, as shown in Fig. 1, the duration of state s_0 corresponds to that of the unperturbed interval between two adjacent IN bursts, which we hence refer to as 'inter-burst time'. By contrast, the duration of state s_1 corresponds to that of an IN burst. Again, the IN considered in this paper is assumed to be asynchronous IN. As the measurement results of [16] demonstrated, both the burst-duration and the unperturbed inter-burst time obey negative exponential distributions. Furthermore, the burst-duration of asynchronous IN is much lower than the inter-burst time. Since the exponential distributions are memoryless [32], the probability density functions (PDFs) of the state-durations t_d conditioned on s_0 and s_1, respectively, can be expressed as

$$f(t_d|s_i) = \frac{1}{\Omega_{s_i,t_d}}\exp\left(-\frac{t_d}{\Omega_{s_i,t_d}}\right), \quad i = 0, 1, \tag{7}$$

where $\Omega_{s_i,t_d} = E[t_d|s_i]$ denotes the conditional expectations of t_d, given s_i for $i = 0, 1$. In addition, we define the ratio of the average burst-duration to the average inter-burst duration (ADIR) as $\Lambda = \Omega_{s_1,t_d}\Omega_{s_0,t_d}$.

Let us assume perfect receiver synchronisation and that the received samples arrive at the time instants of 0, Δt, $2\Delta t$, …, $(M-1)\Delta t$. Let us define the normalised HSMM state-duration as $d = [t_d\Delta t]$, where $[x]$ represents the rounded integer closest to the real value x. Then, the mean of the normalised HSMM state-duration d conditioned on s_0 and s_1 can be calculated as $\Omega_{s_0,d} = \Omega_{s_0,t_d}\Delta t$ and $\Omega_{s_1,d} = \Omega_{s_1,t_d}\Delta t$, respectively. According to Appendix, the probability mass functions (PMFs) of d conditioned on s_0 and s_1 are given by

$$p(d|s_i) = G(d, \Omega_{s_i,d}), \quad i = 0, 1, \tag{8}$$

for $d = 0, 1, \ldots$, where the function $G(x, \Omega)$ is defined in (47).

Let us assume that the initial state of the noise process is chosen from $\{s_0, s_1\}$ with equal probability of 0.5. Then, according to the characteristics of the noise process, as shown in Fig. 1, the states s_0 and s_1 occur alternatively. Hence, the self-transition probabilities of state s_0 and state s_1 are 0, i.e. we have $P_{00} = P_{11} = 0$, where P_{ij} denotes the transition probability from state s_i to state s_j. Therefore, we have the transition probabilities of $P_{01} = P_{10} = 1$. Moreover, when assuming that the noise samples during both states obey the complex-valued Gaussian distributions with a mean of zero and with their individual variances depending on the corresponding state, the PDFs of a noise sample n conditioned on s_0 and s_1 can be expressed as

$$f(n|s_i) = \frac{1}{2\pi\sigma^2_{s_i,n}}\exp\left(-\frac{|n|^2}{2\sigma^2_{s_i,n}}\right), \quad i = 0, 1, \tag{9}$$

where $\sigma^2_{s_i,n}$ denotes the noise variances in state s_i for $i = 0, 1$. In addition, for convenience, we define the ratio of these variances as $\mu = \sigma^2_{s_1,n}\sigma^2_{s_0,n}$.

Above, the proposed noise model has been described in the TD. However, as shown in (4), the detection performance of the OFDM system is affected by the noise samples in the frequency-domain (FD), which are given by $\boldsymbol{N} = \mathcal{F}\boldsymbol{n}$. Therefore, in the following section, we analyse the statistics of the noise in the FD.

3 Statistics of FD noise samples

Recall from our previous discussions that the OFDM symbols are impaired by the noise samples of the state sequence $\hat{\boldsymbol{s}} = \{\hat{s}_1, \hat{s}_2, \ldots, \hat{s}_T\}$, where $\hat{s}_j \in \{s_0, s_1\}$, T denotes the number of noise states encountered during a transmission block and any two consecutive states of $\hat{\boldsymbol{s}}$ satisfy $\hat{s}_j \neq \hat{s}_{j+1}$. Then, as shown in Fig. 2, a TD OFDM symbol may be corrupted by one of three different types of noise. As shown in Fig. 2*a*, the first one is when the M noise samples are all from the same state, either s_0 or s_1. During the second type the noise samples are from a pair of different states $\hat{s}_j$ and $\hat{s}_{j+1}$, namely from s_0 and s_1, as shown in Fig. 2*b*. Finally, during the third type the noise samples are from more than two successive states $\hat{s}_j, \hat{s}_{j+1}, \ldots, \hat{s}_{j+k}$, where $k \geq 2$, as exemplified in Fig. 2*c*. However, in practice, the average inter-arrival time of impulsive bursts is usually much higher than the OFDM symbol duration, i.e. we have $\Omega_{s_0,t_d} \gg T_{\mathrm{s}}$. Hence, for the third type we may only consider the case of $k = 2$ and the scenario of having three successive states s_0, s_1, s_0.

It can be readily shown that in the FD there are also two states, namely S_0 without IN and S_1 representing the presence of IN. Let us define the duration of state S_0 in terms of the number of successive OFDM symbols that are not corrupted by IN, while the duration of state S_1 as the number of successive OFDM symbols impaired by IN. For convenience of analysis, we let η be the number of TD chips spanning from the start of an OFDM symbol to the time instant of a state transition, as shown in Fig. 3. Since η is the offset relative to the start of an OFDM symbol, we can assume that η obeys the discrete uniform distribution having a PMF given by

$$p(\eta) = \frac{1}{M}, \quad \eta = 0, 1, \ldots, M-1. \tag{10}$$

On the basis of the above assumptions, for a given FFT size of M, we can show that when the noise samples in $\boldsymbol{n}$ are generated during state

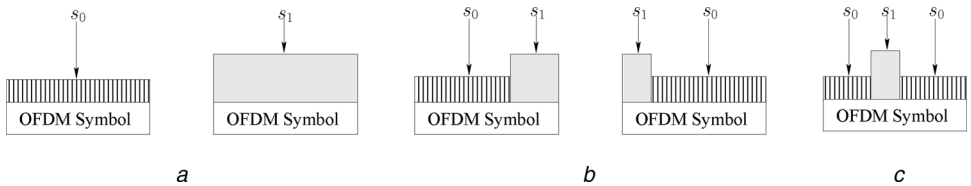

Fig. 2 *Stylised illustration of noise types in the TD*
a–c

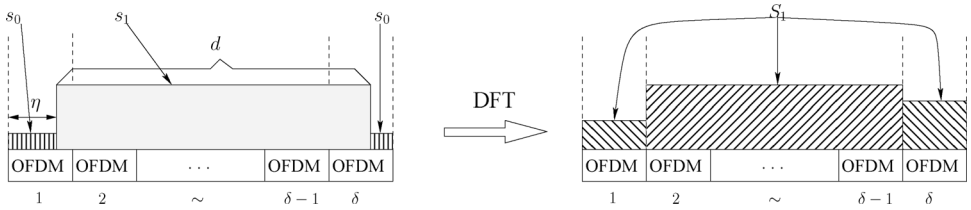

Fig. 3 *Illustration of δ successive OFDM symbols, which are corrupted by noise samples in both the TD and in the corresponding FD*

s_i, where $i \in \{0, 1\}$, with a normalised HSMM state duration of d, the corresponding observations in the FD belong to state S_i with a duration of δ, where for $i \in \{0, 1\}$, δ is given by

$$\delta = \begin{cases} q - 2 + 2i & \text{if } 1 - i \le \eta \le r - 1 + i \\ q - 1 + 2i & \text{if } r + i \le \eta \le M - 1, \\ & \textbf{or } \eta = 0 \text{ for } i = 0 \end{cases} \tag{11}$$

with $q = \lceil dM \rceil$ as well as $r = \lceil dM \rceil M - d$ being positive integers and $\lceil x \rceil$ denotes the smallest integer larger than x. It should be noted that our assumption for the third type of noise in the TD guarantees that δ is always a positive integer.

Furthermore, as shown in Appendix, the PMFs of δ conditioned on S_i, where $i = 0, 1$, are given by

$$p(\delta|S_i) = \Omega_{S_i,\delta}\left[G\left(\frac{\delta + (-1)^i}{2}, \Omega_{S_i,\delta}\right)\right]^2 - \zeta(\Omega_{S_i,\delta}), \quad \delta = 1, 2, \ldots, \tag{12}$$

where $\zeta(\Omega_{S_i}, \delta)$ is defined in (50), $\Omega_{S_0}, \delta = E(\delta|S_0)$ and $\Omega_{S_1}, \delta = E(\delta|S_1)$ denote the expectations of δ, given S_0 and S_1, respectively.

Let the noise samples generated in state S_i with a duration of δ be expressed as $\boldsymbol{N} = \{\boldsymbol{N}(1), \boldsymbol{N}(2), \ldots, \boldsymbol{N}(\delta)\}$, where $\boldsymbol{N}(j) = \mathcal{F}[\boldsymbol{n}(j)]$, and let the number of the samples in $\boldsymbol{n}(j)$ that are from the state s_1 be κ, where $\kappa \in \{0, 1, \ldots, M\}$. As a result, there are $(M - \kappa)$ samples in $\boldsymbol{n}(j)$ generated from the state s_0. Then, we can show that the noise samples in $\boldsymbol{N}(j)$ are complex-valued Gaussian random variables with a mean of zero and a variance given by

$$\sigma^2_{S_i,N}(j) = \frac{(M - \kappa)\sigma^2_{s_0,n} + \kappa\sigma^2_{s_1,n}}{M} = \left[1 + \frac{\kappa(\mu - 1)}{M}\right]\sigma^2_{s_0,n}, \tag{13}$$

where κ is dependent not only on the state S_i but also on the duration δ, which are detailed below.

In the following analysis, we assume that each transmission is sufficiently long for ensuring that the statistical distributions of the durations of the FD states S_0 and S_1 can be described by the PMFs of (12). Furthermore, we can show that during each transmission, we have $|K_0 - K_1| = 1$, where the number of FD states S_i is denoted by K_i. Based on our assumptions, K_0 and K_1 are sufficiently large so that $K_0 K_1 \simeq 1$. Let us denote the kth duration conditioned on state S_i as $\delta_{S_i,k}$, where we have $\sum_{k=1}^{K_i} \delta_{S_i,k} = \Omega_{S_i,\delta} K_i$ for $i = 0$, 1. Hence, for a given FD observation $\widetilde{\boldsymbol{X}}$, which represents the OFDM symbol of (4), the *a posteriori* probability of the OFDM symbol becoming impaired by noise samples generated by the state S_i can be expressed as

$$P(S_i|\widetilde{\boldsymbol{X}}) = \frac{\sum_{k=1}^{K_i} \delta_{S_i,k}}{\sum_{k=1}^{K_0} \delta_{S_0,k} + \sum_{k=1}^{K_1} \delta_{S_1,k}} = \frac{\Omega_{S_i,\delta} K_i}{\Omega_{S_0,\delta} K_0 + \Omega_{S_1,\delta} K_1} \simeq \frac{\Omega_{S_i,\delta}}{\Omega_{S_0,\delta} + \Omega_{S_1,\delta}}. \tag{14}$$

Substituting (45) into (14) gives

$$P(S_i|\widetilde{\boldsymbol{X}}) \simeq \frac{\Lambda^i}{1 + \Lambda}, \tag{15}$$

where Λ was defined in Section 2.3. Then, according to Bayes' rule, we can show that

$$\begin{aligned} P(\delta, S_i|\widetilde{\boldsymbol{X}}) &= \frac{P(\delta, S_i, \widetilde{\boldsymbol{X}})}{P(\widetilde{\boldsymbol{X}})} \\ &= \frac{P(\delta|S_i, \widetilde{\boldsymbol{X}})P(S_i, \widetilde{\boldsymbol{X}})}{P(\widetilde{\boldsymbol{X}})} \\ &= P(\delta|S_i, \widetilde{\boldsymbol{X}})P(S_i|\widetilde{\boldsymbol{X}}), \end{aligned} \tag{16}$$

where $P(\delta|S_i, \widetilde{\boldsymbol{X}})$ is the probability that for a given OFDM symbol impaired by the noise samples generated by the state S_i, this OFDM symbol belongs to that specific set of δ successive OFDM symbols, all of which are impaired by the noise samples generated by the state S_i, as shown in Fig. 3. Let the number of states S_i having a duration of δ successive OFDM symbols in the FD be denoted as k_δ, where we have $\sum_{\delta=1}^{\infty} k_\delta = K_i$. Furthermore, we have $p(\delta|S_i) = k_\delta K_i$. Consequently, it can be shown that

$$\begin{aligned} P(\delta|S_i, \widetilde{\boldsymbol{X}}) &= \frac{\delta k_\delta}{\sum_{k=1}^{K_i} \delta_k} = \frac{\delta k_\delta}{\Omega_{S_i,\delta} K_i} \\ &= \frac{\delta p(\delta|S_i)}{\Omega_{S_i,\delta}}. \end{aligned} \tag{17}$$

Upon substituting (15) and (17) into (16), we arrive at

$$P(\delta, S_i|\widetilde{\boldsymbol{X}}) = \frac{\Lambda^i}{1 + \Lambda} \frac{\delta p(\delta|S_i)}{\Omega_{S_i,\delta}}. \tag{18}$$

Below, we derive the PMF $p(\kappa)$, where κ assumes different values.

3.1 $\kappa = 0$

First, when only the FD state S_0 is encountered during the transmission of δ OFDM symbols, we have $\kappa = 0$. Thus, the probability of $\kappa = 0$ is equal to the probability of an OFDM symbol being impaired by the noise samples generated by S_0, which is given by

$$P(\kappa) = P(S_0|\widetilde{\boldsymbol{X}}) \simeq \frac{1}{1 + \Lambda}, \quad \kappa = 0. \tag{19}$$

3.2 $\kappa = 1, 2, \ldots, M - 1$

Second, as shown in Fig. 3, if the FD state S_1 having a duration of $\delta \ge 2$ occurs, we may have $1 \le \kappa \le M - 1$ [Here, κ maybe equal to M. However, recalling our assumptions that the transmission time is long enough and M is sufficiently large, the case where

state S_1 with a duration of $\delta \geq 2$ and $\kappa = M$ for $j = 1$ occurs rarely. Thus, in our analysis, the probability of this special case is negligible.], when the first and the last (δth) OFDM symbols are considered. Therefore, we have

$$\Pr_1(1 \leq \kappa \leq M-1) = \sum_{\delta=2}^{\infty} \frac{2}{\delta} P(\delta, S_1|\widetilde{\boldsymbol{X}}), \tag{20}$$

where 2δ is the probability of the first and the last (δth) OFDM symbols being picked from the δ consecutive OFDM symbols. Furthermore, with the aid of (18) and (46a), we arrive at

$$\begin{aligned}\Pr_1(1 \leq \kappa \leq M-1) &= \frac{\Lambda}{1+\Lambda} \frac{2\sum_{\delta=2}^{\infty} p(\delta|S_1)}{\Omega_{S_1,\delta}} \\ &= \frac{2\Lambda}{1+\Lambda}\left[\frac{1}{\Omega_{S_1,\delta}} - 1 + G(0.5, \Omega_{S_1,\delta})\right],\end{aligned} \tag{21}$$

where $G(x, \Omega)$ is defined in (47).

As shown in Fig. 2*b*, we have $\kappa = (M - \eta)$ and η obeys the uniform distribution. Therefore, we have

$$\begin{aligned}P_1(\kappa) &= \frac{1}{M-1}\Pr_1(1 \leq \kappa \leq M-1) \\ &= \frac{\Lambda}{1+\Lambda}\frac{2}{M-1}\left[\frac{1}{\Omega_{S_1,\delta}} - 1 + G(0.5, \Omega_{S_1,\delta})\right] \\ &= \frac{\Lambda}{1+\Lambda}\left[\frac{(2/\Omega_{S_1,\delta}) + 2G(0.5, \Omega_{S_1,\delta}) - 2}{(M-1)}\right]\end{aligned} \tag{22}$$

for $\kappa = 1, 2, \ldots, M-1$. Equation (22) shows that $P_1(\kappa)$ is independent of κ.

On the other hand, when the FD state S_1 with a duration of $\delta = 1$ occurs, we may also have $1 \leq \kappa \leq M-1$. In this case, as shown in Fig. 2*c*, we have $\kappa = d$. Thus, by substituting (43a) into (18), we can show that

$$\begin{aligned}&\Pr_2(1 \leq \kappa \leq M-1) \\ &\quad = \sum_{\kappa=1}^{M-1} \frac{\Lambda}{1+\Lambda} \frac{(M-\kappa+1)G(\kappa, \Omega_{s_1,d})}{\Omega_{s_1,d}}.\end{aligned} \tag{23}$$

In this case, we find that the distribution of κ obeys the PMF $G(\kappa, \Omega_{s_1,d})$. Thus, we can write

$$P_2(\kappa) = \frac{\Lambda}{1+\Lambda} \frac{(M-\kappa+1)G(\kappa, \Omega_{s_1,d})}{\Omega_{s_1,d}}, \tag{24}$$

for $\kappa = 1, 2, \ldots, M-1$.

Consequently, the probability of $\kappa = 1, 2, \ldots, M-1$ can be obtained by considering both of the above cases, yielding

$$\begin{aligned}P(\kappa) &= P_1(\kappa) + P_2(\kappa) \\ &= \frac{\Lambda}{1+\Lambda}\left[\frac{(2/\Omega_{S_1,\delta}) + 2G(0.5, \Omega_{S_1,\delta}) - 2}{(M-1)} \right. \\ &\quad \left. + \frac{(M-\kappa+1)G(\kappa, \Omega_{s_1,d})}{\Omega_{s_1,d}}\right],\end{aligned} \tag{25}$$

for $\kappa = 1, 2, \ldots, M-1$.

3.3 $\kappa = M$

As shown in Fig. 3, when the FD state S_1 with a duration of $\delta \geq 2$ occurs, we have $\kappa = M$ for the jth, $j \in \{2, \ldots, \delta - 1\}$, OFDM symbols. Therefore, we arrive at

$$P(\kappa) = \sum_{\delta=2}^{\infty} \frac{\delta - 2}{\delta} P(\delta, S_1|\widetilde{\boldsymbol{X}}), \quad \kappa = M. \tag{26}$$

Upon substituting (18) into the above equation, we obtain

$$\begin{aligned}P(\kappa) &= \frac{\Lambda}{1+\Lambda} \frac{\sum_{\delta=2}^{\infty} \delta p(\delta|S_1) - 2\sum_{\delta=2}^{\infty} p(\delta|S_1)}{\Omega_{S_1,\delta}} \\ &= \frac{\Lambda}{1+\Lambda}\left[2 - \frac{2}{\Omega_{S_1,\delta}} - G(0.5, \Omega_{S_1,\delta})\right],\end{aligned} \tag{27}$$

for $\kappa = M$.

In summary, the PMF of κ is given in the following equation (see (28))

4 Analysis of the average BER

In this section, we first analyse the signal-to-noise ratio (SNR) based on our noise model. Then, a closed-form formula is derived for the average BER of the OFDM-modulated PLC system.

4.1 SNR analysis

According to (4) and (13), the instantaneous SNR per symbol for the ith subchannel is given by

$$\begin{aligned}\gamma_{i,\kappa} &= \frac{|H_i|^2 E_s}{\left[1 + (\mu - 1)(\kappa/M)\right]\sigma^2_{s_0,n}} \\ &= \frac{|H_i|^2}{1 + (\mu - 1)(\kappa/M)} \times \gamma_{s_0,n},\end{aligned} \tag{29}$$

where H_i is the fading gain of the ith subchannel, E_s is the signal energy per symbol and, by definition, $\gamma_{s_0,n} = E_s\sigma^2_{s_0,n}$ denotes the SNR encountered in state s_0. Equation (29) shows that $\gamma_{i,\kappa}$ depends on both the channel fading and on the time-variant noise power. As mentioned in Section 2.2, the PLC channel can be assumed to be time-invariant during an OFDM symbol. Thus, the

$$p(\kappa) = \begin{cases} \dfrac{1}{1+\Lambda}, & \kappa = 0 \\ \dfrac{\Lambda}{1+\Lambda}\left[\dfrac{(2/\Omega_{S_1,\delta}) + 2G(0.5, \Omega_{S_1,\delta}) - 2}{(M-1)} + \dfrac{(M-\kappa+1)G(\kappa, \Omega_{s_1,d})}{\Omega_{s_1,d}}\right], & \kappa = 1, 2, \ldots, M-1 \\ \dfrac{\Lambda}{\Lambda+1}\left[2 - \dfrac{2}{\Omega_{S_1,\delta}} - G(0.5, \Omega_{S_1,\delta})\right], & \kappa = M. \end{cases} \tag{28}$$

Table 1 Parameters $[\rho_l, \theta_l]$ for different modems

	BPSK	QPSK	16QAM	64QAM
$[\rho_1, \theta_1]$	$[1, \sqrt{2}]$	[1,1]	$\left[\frac{3}{4}, \sqrt{\frac{1}{5}}\right]$	$\left[\frac{7}{12}, \sqrt{\frac{1}{21}}\right]$
$[\rho_2, \theta_2]$	–	–	$\left[\frac{1}{2}, 3\sqrt{\frac{1}{5}}\right]$	$\left[\frac{1}{2}, 3\sqrt{\frac{1}{21}}\right]$
$[\rho_3, \theta_3]$	–	–	$\left[-\frac{1}{4}, 5\sqrt{\frac{1}{5}}\right]$	$\left[-\frac{1}{12}, 5\sqrt{\frac{1}{21}}\right]$
$[\rho_4, \theta_4]$	–	–	–	$\left[\frac{1}{12}, 9\sqrt{\frac{1}{21}}\right]$
$[\rho_5, \theta_5]$	–	–	–	$\left[-\frac{1}{12}, 13\sqrt{\frac{1}{21}}\right]$

fading gain of all the subchannels is the same during the transmission of an OFDM. However, κ is a random variable with the PMF given by (28).

4.2 Average BER

Given the SNR, the average BER of the OFDM-assisted PLC system can be obtained by averaging the conditional BER $P_e(\gamma_{i,\kappa})$ over the distribution of the SNR $\gamma_{i,\kappa}$, which is expressed as

$$P_b = \frac{1}{M}\sum_{i=0}^{M-1}\sum_{\kappa=0}^{M} P_e(\gamma_{i,\kappa})p(\kappa), \tag{30}$$

where $p(\kappa)$ is given in (28). In (30), $P_e(\gamma_{i,k})$ is the BER of Q-ary QAM employing Gray coding for a given SNR $\gamma_{i,\kappa}$, which can be expressed in a generalised form as [33, 34]

$$P_e(\gamma_{i,\kappa}) = \sum_l \rho_l Q(\theta_l\sqrt{\gamma_{i,\kappa}}), \tag{31}$$

where $Q(x) = (1/\sqrt{2\pi})\int_x^\infty \mathrm{e}^{-t^2/2}\,\mathrm{d}t$ is the Gaussian Q-function, while the values of ρ_l and θ_l for the different modulation schemes are given in Table 1. Finally, upon substituting (28) and (31) into (30), the average BER of the OFDM-assisted PLC system under our noise model can be shown in the following equation:

$$\begin{aligned} P_b = {} & \frac{1}{M(1+\Lambda)}\sum_{i=0}^{M-1}\Bigg\{P_e\left(|H_i|^2\gamma_{s_0,n}\right) + \frac{\Lambda}{\Omega_{s_1,d}} \\ & \sum_{\kappa=1}^{M-1}(M-\kappa+1)G(\kappa, \Omega_{s_1,d})P_e\left(\frac{|H_i|^2}{1+(\mu-1)(\kappa/M)}\gamma_{s_0,n}\right) \\ & + \Lambda\left[\frac{(2/\Omega_{S_1,\delta}) + 2G(0.5, \Omega_{S_1,\delta}) - 2}{(M-1)}\right] \\ & \sum_{\kappa=1}^{M-1} P_e\left(\frac{|H_i|^2}{1+(\mu-1)(\kappa/M)}\gamma_{s_0,n}\right) \\ & + \Lambda\left[2 - \frac{2}{\Omega_{S_1,\delta}} - G(0.5, \Omega_{S_1,\delta})\right]P_e\left(\frac{|H_i|^2}{\mu}\gamma_{s_0,n}\right)\Bigg\}. \end{aligned} \tag{32}$$

Table 2 4-path channel model [8]

	$\alpha(f) = 0.78f$ (ns Hz/m), $v_p = 2\times10^8$ m/s			
l	1	2	3	4
g_i	0.6400	0.3800	−0.1500	0.0500
τ_i, μs	1.0000	1.1120	1.2240	1.3375

5 Performance results

In this section, the BER performance of OFDM-assisted PLC systems is evaluated by comparing the analytical and simulation results for a bandwidth of 25 MHz. A sampling frequency of 50 MHz is used for meeting the Nyquist criterion, which leads to the chip duration of 20 ns. For the indoor PLC channels, the 4-path model of [8] is employed and the corresponding parameters are given in Table 2, while the corresponding CTF is shown in Fig. 4. In the FD, the correlation coefficient of the CTF can be expressed as

$$R_{\Delta f} = \frac{E[H(f)H^*(f+\Delta f)]}{E[|H(f)|^2]}, \tag{33}$$

where $H(f)$ is given in (5) and $H^*(f)$ denotes the conjugate of $H(f)$. Upon substituting the parameters of Table 2 into (5), the 90% coherence bandwidth of the channel can be obtained with the aid of (33), which is equal to 588.24 kHz. In order to guarantee that each OFDM subchannel exhibits flat fading, the number of subcarriers of the OFDM system should satisfy $M \gg (25\ \text{MHz}/0.58824\ \text{MHz}) \simeq 42.5$. Hence, in our studies, we opted for $M = 256$. In addition, in order to avoid the ISI, the length of the CP is chosen to be $L' = 50$, which leads to $L'\Delta t > \tau_{\max}$.

The measurement results of [16] show that the average duration of the IN in PLCs is about $\Omega_{s_1,t_d} = 60\,\mu\text{s}$ for typical and weak impairments, which are used in our simulations, while the average inter-arrival time varies from a few seconds to a few milliseconds in practical scenarios. In order to increase the associated flexibility, the ADIR Λ defined in Section 2.3 is varied in order to obtain different average inter-arrival times. For a non-dispersive channel we let $L' = 0$ and $H_i = 1$ for $i = 0, 1, \ldots, M-1$.

We infer from the above discussions that in order to mitigate the ISI, the length of CP is chosen to be 50 samples in our simulations, hence the system's normalised transmission rate is reduced to $M(M+L') \simeq 0.837$, which results in about 0.77 dB loss of SNR. Observe from (29) that the SNR is jointly determined by both the CTF and the IN, which is characterised by the parameter μ. Since the CTF is independent of the noise, we may analyse their effects on the system's performance separately.

In Fig. 5, we study the BER performance of the OFDM system considered, when communicating over either non-dispersive additive white Gaussian noise (AWGN) channels or over dispersive PLC channels subjected to both IN and AWGN. In this figure, four different modulation schemes are considered, which are BPSK, QPSK, 16QAM and 64QAM. In addition to the well-understood classic features of the different modulation schemes, from the results of Fig. 5 we infer the following observations. First, when the PLC channels become dispersive, the

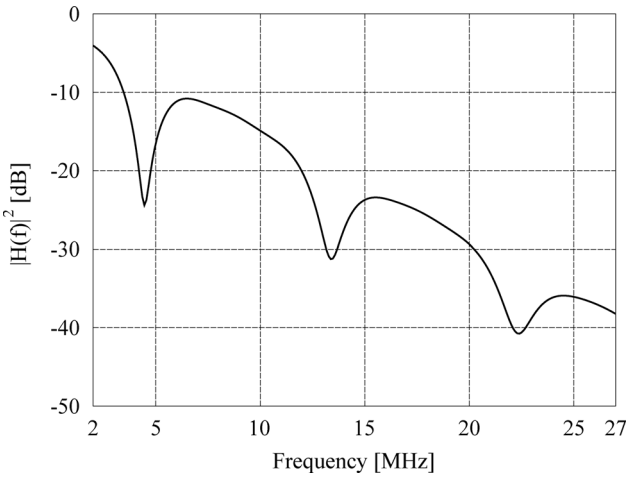

Fig. 4 *4-path model of the indoor PLC channel of [8]. Corresponding channel parameters are given in Table 2*

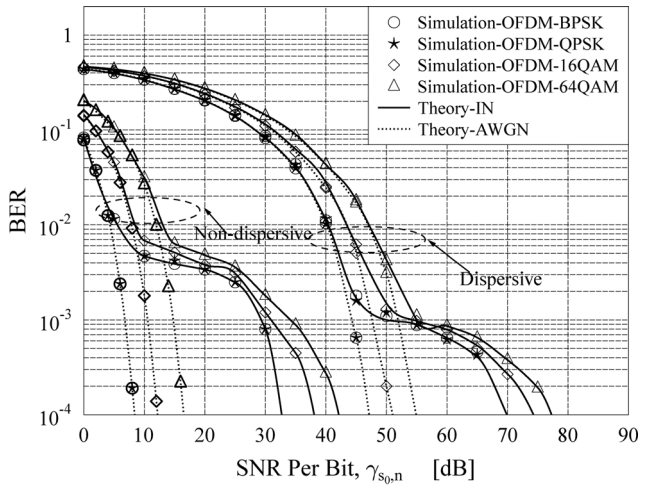

Fig. 5 *BER performance of OFDM systems associated with $M = 256$ and $L' = 50$ using BPSK, QPSK, 16QAM, or 64QAM when communicating over either non-dispersive AWGN channels or dispersive PLC channels contaminated both by IN and AWGN. Average inter-arrival time of the IN bursts is $\Omega_{s_0,t_d} = 6$ ms, the average duration of the IN bursts is $\Omega_{s_1,t_d} = 60\,\mu$s, and the ratio between the IN power and the background noise power is $\mu = 30$ dB*

BER performance significantly degrades. As shown in Fig. 5, for a given BER of 10^{-4}, communicating over dispersive PLC channels requires as much as 40 dB higher SNR $\gamma_{s_0,n}$ than communicating over non-dispersive AWGN channels. This performance loss may be explained with the aid of Fig. 4, where the deep fades of the channel may reach 40 dB attenuation, hence the BER is severely degraded. Second, the impulse noise also severely affects the achievable BER performance. As shown in Fig. 5, when the PLC channels experience both IN and AWGN, marked as 'Theory-IN', about 25 dB of SNR loss is observed in comparison to the PLC channels experiencing only AWGN.

In Fig. 6, we investigate the effect of ADIR on the BER performance of OFDM-based PLC systems having $M = 256$ subcarriers and a CP length of $L' = 0$, when communicating over non-dispersive channels subjected to both IN and AWGN. In this figure, only BPSK is considered, but the BER curves of the higher-order Q-ary QAM obey similar tendencies. In comparison to the channels experiencing only AWGN, when the channels

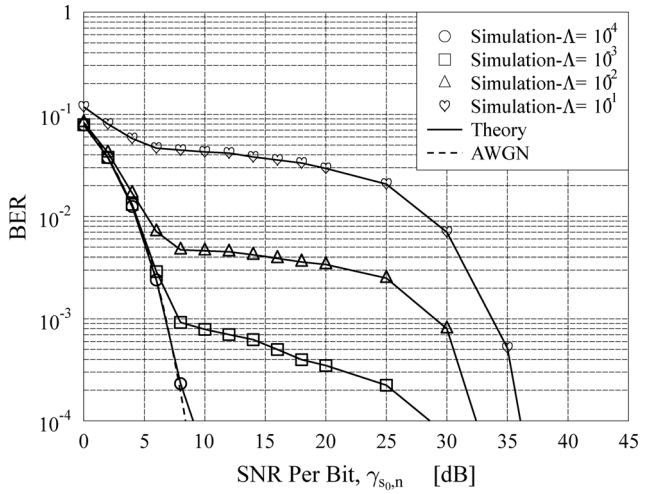

Fig. 6 *BER performance of the OFDM system for $M = 256$ and $L' = 0$ using BPSK, when communicating over a non-dispersive channel subjected to both IN and AWGN. Average duration of bursts is $\Omega_{s_1,t_d} = 60\,\mu$s, while the average inter-arrival time varies with the value of the ADIR Λ. Ratio between the IN power and the background noise power is $\mu = 30$ dB*

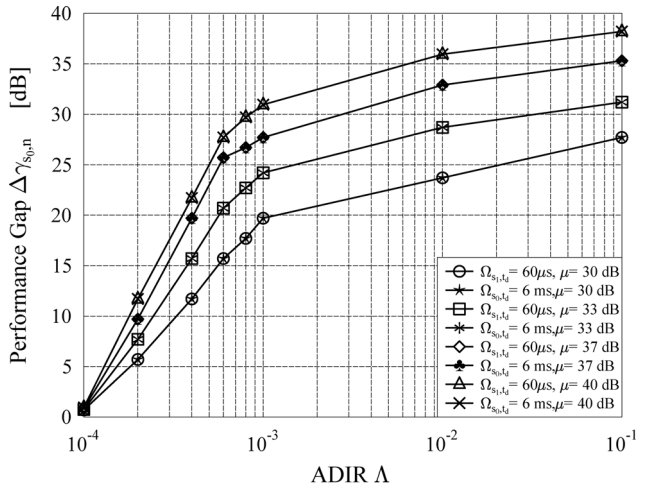

Fig. 7 *Performance gap $\Delta\gamma_{s_0,n}$ per bit against the ADIR Λ at a BER of 10^{-4}. OFDM system relies on $M = 256$ and $L' = 0$ using BPSK, when communicating over a non-dispersive channel subjected to both IN and AWGN*

experience both IN and AWGN, there is a gradual slope change for the BER curve at a certain value of SNR, as shown in Fig. 6. This implies that before this point the system performance is dominated by the AWGN, and then more and more by the IN. As a result of IN, the system's performance is degraded predominantly depending on the value of ADIR. When the ADIR is increased, the system performance degradation becomes more severe, because according to (32), the probability of an OFDM symbol becoming impaired by high-power IN bursts increases.

In Fig. 7, we show the effect of ADIR on the performance gap $\Delta\gamma_{s_0,n}$ between the channels experiencing AWGN alone and the channels experiencing both IN as well as AWGN at a BER of 10^{-4}. First, according to the definition of the ADIR in Section 2.3, we can change the value of Λ either by keeping Ω_{s_1,t_d} constant and changing Ω_{s_0,t_d}, or by keeping Ω_{s_0,t_d} constant, but varying Ω_{s_1,t_d}. As shown in Fig. 7, when Λ varies from 10^{-4} to 10^{-1}, the performance results associated with keeping Ω_{s_1,t_d} constant are the same as those of keeping Ω_{s_0,t_d} constant. Second, observe in Fig. 7 that when the ADIR increases, the performance gap gradually increases, but asymptotically tending to a certain value. This observation can be explained with the aid of (32), which shows that as the value of Λ becomes larger, the performance becomes similar to that of the system, where the channels experience only AWGN with a variance of $\mu\sigma^2_{s_0,n}$.

6 Conclusions

In this paper, a HSMM was invoked for representing the statistical properties of the asynchronous IN encountered in PLC channels. A closed-form BER expression has been derived for the OFDM system communicating over dispersive indoor PLC channels experiencing both background and asynchronous IN. The accuracy of our analytical results has been verified by our simulation results. Furthermore, the BER performance has been investigated for different scenarios both numerically and by simulations. We have shown that the system performance is severely degraded by the CTF of PLC channels, which is aggravated by the asynchronous IN. Therefore, the effect of asynchronous IN has to be mitigated by efficient techniques, which will be the subject of our future research.

7 Acknowledgments

The financial support of the European Research Council's (ERC) Advanced Fellow Grant was gratefully acknowledged.

8 References

1 Hrasnica, H., Haidine, A., Lehnert, R.: 'Broadband powerline communications: network design' (Wiley, 2005)
2 Galli, S., Scaglione, A., Wang, Z.: 'For the grid and through the grid: The role of power line communications in the smart grid', *Proc. IEEE*, 2011, **99**, (6), pp. 998–1027
3 Ma, Y.H., So, P., Gunawan, E.: 'Performance analysis of OFDM systems for broadband power line communications under impulsive noise and multipath effects', *IEEE Trans. Power Deliv.*, 2005, **20**, (2), pp. 674–682
4 'IEEE Standard for Broadband over Power Line Networks: Medium Access Control and Physical Layer Specifications', *IEEE Std 1901–2010*, 2010, pp. 1–1586
5 HomePlug AV2 White Paper. HomePlug Powerline Alliance. Available as: http://www.homeplug.org/
6 I.-T. R. G.9960: '*Unified high-speed wireline-based home networking transceivers-system architecture and physical layer specification*', 2011
7 Ferreira, H.C., Lampe, L., Newbury, J., Swart, T.G. (Eds.): 'Power line communications: theory and applications for narrowband and broadband communications over power lines' (Wiley-Blackwell, 2010, 1st edn.)
8 Zimmermann, M., Dostert, K.: 'A multipath model for the powerline channel', *IEEE Trans. Commun.*, 2002, **50**, (4), pp. 553–559
9 Anastasiadou, D., Antonakopoulos, T.: 'Multipath characterization of indoor power-line networks', *IEEE Trans. Power Deliv.*, 2005, **20**, (1), pp. 90–99
10 Galli, S., Banwell, T.: 'A deterministic frequency-domain model for the indoor power line transfer function', *IEEE J. Sel. Areas Commun.*, 2006, **24**, (7), pp. 1304–1316
11 Tlich, M., Zeddam, A., Moulin, F., *et al.*: 'Indoor power-line communications channel characterization up to 100 MHz – Part II: Time–frequency analysis', *IEEE Trans. Power Deliv.*, 2008, **23**, (3), pp. 1402–1409
12 Galli, S.: 'A simplified model for the indoor power line channel'. IEEE Int. Symp. on Power Line Communications and its Applications, 2009, ISPLC 2009, March 2009, pp. 13–19
13 Tonello, A., Versolatto, F.: 'Bottom-up statistical PLC channel modeling – Part II: Inferring the statistics', *IEEE Trans. Power Deliv.*, 2010, **25**, (4), pp. 2356–2363
14 Galli, S.: 'A novel approach to the statistical modeling of wireline channels', *IEEE Trans. Commun.*, 2011, **59**, (5), pp. 1332–1345
15 Tonello, A., Versolatto, F., Béjar, B., *et al.*: 'A fitting algorithm for random modeling the PLC channel', *IEEE Trans. Power Deliv.*, 2012, **27**, (3), pp. 1477–1484
16 Zimmermann, M., Dostert, K.: 'Analysis and modeling of impulsive noise in broad-band powerline communications', *IEEE Trans. Electromagn. Compat.*, 2002, **44**, (1), pp. 249–258
17 Meng, H., Guan, Y., Chen, S.: 'Modeling and analysis of noise effects on broadband power-line communications', *IEEE Trans. Power Deliv.*, 2005, **20**, (2), pp. 630–637
18 Channel Model Sub-committee of P1901: 'Electrical network and topology channel and noise model'. P1901-10-0356-00, Tech. Rep., September 2010
19 FP7 Theme 3 ICT-213311 OMEGA: 'PLC channel characteriztion and modelling'. Tech. Rep., December 2008
20 Blackard, K., Rappaport, T., Bostian, C.: 'Measurements and models of radio frequency impulsive noise for indoor wireless communications', *IEEE J. Sel. Areas Commun.*, 1993, **11**, (7), pp. 991–1001
21 Kassam, S.A.: 'Signal detection in non-Gaussian noise' (Springer-Verlag, 1988)
22 Ghosh, M.: 'Analysis of the effect of impulse noise on multicarrier and single carrier QAM systems', *IEEE Trans. Commun.*, 1996, **44**, (2), pp. 145–147
23 Middleton, D.: 'Non-Gaussian noise models in signal processing for telecommunications: new methods and results for class A and class B noise models', *IEEE Trans. Inf. Theory*, 1999, **45**, (4), pp. 1129–1149
24 Amirshahi, P., Navidpour, S., Kavehrad, M.: 'Performance analysis of uncoded and coded OFDM broadband transmission over low voltage power-line channels with impulsive noise', *IEEE Trans. Power Deliv.*, 2006, **21**, (4), pp. 1927–1934
25 Fertonani, D., Colavolpe, G.: 'On reliable communications over channels impaired by bursty impulse noise', *IEEE Trans. Commun.*, 2009, **57**, (7), pp. 2024–2030
26 Ndo, G., Labeau, F., Kassouf, M.: 'A Markov-Middleton model for bursty impulsive noise: modeling and receiver design', *IEEE Trans. Power Deliv.*, 2013, **28**, (4), pp. 2317–2325
27 Levinson, S.E.: 'Continuously variable duration hidden Markov models for automatic speech recognition', *Comput. Speech Lang.*, 1986, **1**, (1), pp. 29–45
28 Yu, S.-Z.: 'Hidden semi-Markov models', *Artif. Intell*, 2009, **174**, (2), pp. 215–243
29 Yang, L.-L.: 'Multicarrier communications' (John Wiley & Sons, Ltd, 2009)
30 Hanzo, L., Ng, S.X., Webb, W.T., *et al.*: 'Quadrature amplitude modulation: from basics to adaptive trellis-coded, turbo-equalised and space-time coded OFDM, CDMA and MC-CDMA systems' (IEEE Press-John Wiley, 2004)
31 Rabiner, L.: 'A tutorial on hidden Markov models and selected applications in speech recognition', *Proc. IEEE*, 1989, **77**, (2), pp. 257–286
32 Bertsekas, D., Gallager, R.: 'Data networks' (Prentice-Hall, 1992)
33 Yang, L.-L., Hanzo, L.: 'A recursive algorithm for the error probability evaluation of M-QAM', *IEEE Commun. Lett.*, 2000, **4**, (10), pp. 304–306
34 Vitthaladevuni, P., Alouini, M.-S.: 'A recursive algorithm for the exact BER computation of generalized hierarchical QAM constellations', *IEEE Trans. Inf. Theory*, 2003, **49**, (1), pp. 297–307
35 Zimmermann, M., Dostert, K.: 'An analysis of the broadband noise scenario in powerline networks'. Proc. ISPLC, April 2000, pp. 131–138
36 Abramowitz, M., Stegun, I.A. (Eds.): 'Handbook of mathematical functions with formulas, graphs, and mathematical tables' (Dover Publications, New York, 1972)
37 Chariag, D., Guezgouz, D., Le Bunetel, J.C., *et al.*: 'Modeling and simulation of temporal variation of channel and noise in indoor power-line network', *IEEE Trans. Power Deliv.*, 2012, **27**, (4), pp. 1800–1808

9 Appendices: derivation of $p(d|s_i)$ and $p(\delta|S_i)$

This Appendix derives the PMFs of d conditioned on s_0 and s_1, as well as the PMFs of δ conditioned on S_0 and S_1.

First, it can be shown that for a given state s_i, where $i = 0, 1$, we have

$$\begin{aligned} p(d|s_i) &= \int_{(d-0.5)\Delta t}^{(d+0.5)\Delta t} \frac{1}{\Omega_{s_i,t_d}} \exp\left(-\frac{t_d}{\Omega_{s_i,t_d}}\right) \mathrm{d}t_d \\ &= \exp\left(-\frac{(d-0.5)\Delta t}{\Omega_{s_i,t_d}}\right) - \exp\left(-\frac{(d+0.5)\Delta t}{\Omega_{s_i,t_d}}\right) \\ &= \exp\left(-\frac{d-0.5}{\Omega_{s_i,d}}\right) - \exp\left(-\frac{d+0.5}{\Omega_{s_i,d}}\right). \end{aligned} \tag{34}$$

Then, according to (8), we can show that

$$\sum_{d=x_1}^{x_2} p(d|s_i) = \exp\left(-\frac{x_1-0.5}{\Omega_{s_i,d}}\right) - \exp\left(-\frac{x_2+0.5}{\Omega_{s_i,d}}\right); \tag{35}$$

$$\begin{aligned} \sum_{d=x_1}^{x_2} dp(d|s_i) &= \Omega_{s_i,d} \exp\left(-\frac{x_1+0.5}{\Omega_{s_i,d}}\right) \\ &\quad - \Omega_{s_i,d} \exp\left(-\frac{x_2-0.5}{\Omega_{s_i,d}}\right) \\ &\quad + x_1 \exp\left(-\frac{x_1-0.5}{\Omega_{s_i,d}}\right) - x_2 \exp\left(-\frac{x_2+0.5}{\Omega_{s_i,d}}\right); \end{aligned} \tag{36}$$

For the state S_0, we can rewrite (11) as

$$\delta = \begin{cases} q-2 & \text{if } 1 \le \eta \le r-1 \\ q-1 & \text{if } r \le \eta \le M-1 \quad \text{and} \quad \eta = 0 \end{cases}, \tag{37}$$

where we have $q = \lceil dM \rceil$ and $r = \lceil dM \rceil M - d$, while $\lceil x \rceil$ denotes the smallest integer not smaller than x. Since d and η are independent, with the aid of (8) and (10), we have

$$\begin{aligned} p(\delta|S_0) &= \sum_{d=(\delta+1)M}^{(\delta+2)M} \frac{(\delta+2)M-d-1}{M} p(d|s_0) \\ &\quad + \sum_{d=\delta M}^{(\delta+1)M} \frac{d-\delta M+1}{M} p(d|s_0) \\ &\simeq \frac{\Omega_{s_0,d}+1}{M} \left[\exp\left(-\frac{\delta M}{\Omega_{s_0,d}}\right) - 2\exp\left(-\frac{(\delta+1)M}{\Omega_{s_0,d}}\right) \right. \\ &\quad \left. + \exp\left(-\frac{(\delta+2)M}{\Omega_{s_0,d}}\right) \right], \end{aligned} \tag{38}$$

where the mean of δ conditioned on S_0 can be calculated as

$$\Omega_{S_0,\delta} = \sum_{\delta=1}^{\infty} \delta p(\delta|S_0) = \frac{\Omega_{s_0,d}+1}{M} \exp\left(-\frac{M}{\Omega_{s_0,d}}\right). \tag{39}$$

In practice, we usually have $\Omega_{s_0,t_d} \gg T_s$. As a result, we have $\Omega_{s_0,d} \gg M$. Thus, we may exploit the following approximation

$$\Omega_{S_0,\delta} \simeq \frac{\Omega_{s_0,d}+1}{M} \simeq \frac{\Omega_{s_0,d}}{M}. \tag{40}$$

Consequently, when substituting (40) into (38), we obtain

$$p(\delta|S_0) \simeq \Omega_{S_0,\delta} \left[\exp\left(-\frac{\delta}{\Omega_{S_0,\delta}}\right) - 2\exp\left(-\frac{\delta+1}{\Omega_{S_0,\delta}}\right) + \exp\left(-\frac{\delta+2}{\Omega_{S_0,\delta}}\right)\right]. \quad (41)$$

For the state S_1, we can rewrite (11) as

$$\delta = \begin{cases} q & \text{if } 0 \le \eta \le r \\ q+1 & \text{if } r+1 \le \eta \le M-1 \end{cases}, \quad (42)$$

where the variables have the same meaning as those in (37). Similarly to (38), with the aid of (8) and (10), we have

$$p(\delta|S_1) = \sum_{d=0}^{M} \frac{M-d+1}{M} p(d|s_1) \simeq \frac{\Omega_{s_1,d}-1}{M}\exp\left(-\frac{M}{\Omega_{s_1,d}}\right), \quad \delta = 1, \quad (43a)$$

and

$$p(\delta|S_1) = \sum_{d=(\delta-1)M}^{\delta M} \frac{\delta M - d + 1}{M} p(d|s_1) + \sum_{d=(\delta-2)M}^{(\delta-1)M} \frac{d-(\delta-2)M-1}{M} p(d|s_1) \simeq \frac{\Omega_{s_1,d}-1}{M}\left[\exp\left(-\frac{(\delta-2)M}{\Omega_{s_1,d}}\right) - 2\exp\left(-\frac{(\delta-1)M}{\Omega_{s_1,d}}\right) + \exp\left(-\frac{\delta M}{\Omega_{s_1,d}}\right)\right], \quad \delta = 2, 3, \ldots. \quad (43b)$$

Similar to (39) and (40), the mean of δ conditioned on S_1 can be calculated as

$$\Omega_{S_1,\delta} = \sum_{\delta=1}^{\infty} \delta p(\delta|S_1) \simeq \frac{\Omega_{s_1,d}}{M}. \quad (44)$$

In addition, the relationship between $\Omega_{S_{1,\delta}}$ and $\Omega_{S_0,\delta}$ can be expressed as

$$\frac{\Omega_{S_1,\delta}}{\Omega_{S_0,\delta}} = \frac{\Omega_{s_1,d}}{\Omega_{s_0,d}} = \Lambda \quad (45)$$

Then, upon substituting (44) into (43a) and (43b), gives

$$p(\delta|S_1) \simeq \Omega_{S_1,\delta}\exp\left(-\frac{1}{\Omega_{S_1,\delta}}\right), \quad \delta = 1, \quad (46a)$$

and

$$p(\delta|S_1) \simeq \Omega_{S_1,\delta}\left[\exp\left(-\frac{\delta-2}{\Omega_{S_1,\delta}}\right) - 2\exp\left(-\frac{\delta-1}{\Omega_{S_1,\delta}}\right) + \exp\left(-\frac{\delta}{\Omega_{S_1,\delta}}\right)\right], \quad \delta = 2, 3, \ldots. \quad (46b)$$

Furthermore, let us define

$$G(x, \Omega) = \exp\left(-\frac{x-0.5}{\Omega}\right) - \exp\left(-\frac{x+0.5}{\Omega}\right) \quad (47)$$

Then, (46b) can be rewritten as

$$p(d|s_i) = G(d, \Omega_{s_i,d}) \quad (48)$$

$$p(\delta|S_i) = \Omega_{S_i,\delta}\left[G\left(\frac{\delta+(-1)^i}{2}, \Omega_{S_i,\delta}\right)\right]^2 - \zeta(\Omega_{S_i,\delta}), \quad (49)$$

where

$$\zeta(\Omega_{S_i,\delta}) = \begin{cases} \Omega_{S_i,\delta}\left[e^{(1/\Omega_{S_i,\delta})} - 2\right] & \text{if } \delta = 1 \text{ and } i = 1 \\ 0 & \text{otherwise} \end{cases} \quad (50)$$

COM20150702

Author Queries

Hongming Zhang, Lie-Liang Yang, Lajos Hanzo

Q1 Please confirm the changes made in the article title.

Q2 Please check the email address of the corresponding author.

Q3 Footnote has been moved to text as required by journal style. Please check and confirm that it has been located correctly within the text.

Q4 References [35–37] are listed in the reference list but not cited in the text. Please cite in the text, else delete from the list.

Q5 Please provide a description for the part labels a–c in Fig. 2.